Marine and Petroleum Geology 127 (2021) 104965

Contents lists available at ScienceDirect

Marine and Petroleum Geology

journal homepage: www.elsevier.com/locate/marpetgeo

Research paper

Effect of sediment source on source rock hydrocarbon potential; An example from the Kimmeridgian and Tithonian-aged source rocks of the central ridge, off-shore Newfoundland, Canada

John B. Gordon [a,b,*], Hamed Sanei [c], Omid H. Ardakani [d,b], Per K. Pedersen [b]

[a] Husky Energy, 707 8th Avenue SW Calgary, AB T2P 3G7, Canada
[b] Department of Geoscience, University of Calgary, 2500 University Drive NW Calgary, AB T2N 1N4, Canada
[c] Lithospheric Organic Carbon (LOC) Group, Department of Geoscience, Aarhus University, Høegh-Guldbergs Gade 2, building 1671, 223, 8000, Aarhus C, Denmark
[d] Natural Resources Canada, Geological Survey of Canada, 3303 33rd St. NW Calgary, AB T2L 2A7, Canada

ARTICLE INFO

Keywords:
Central ridge offshore newfoundland
Red green quotient
Organic petrology
Organic geochemistry
Thermal maturity

ABSTRACT

This study presents an integrated approach using organic geochemistry and incident-light organic petrographic microscopy techniques to characterize kerogen type, hydrocarbon potential, thermal maturity, and the effect depositional environment has on five wells from Upper-Jurassic Kimmeridgian and Tithonian-aged source rock intervals in the Central Ridge area offshore Newfoundland, Canada. The results show that hydrocarbon potential in these organic-rich marine mudrocks is mainly dependent on depositional environment and present-day burial depth of the sediments. Oscillations and transitions between (i) rocks with dominant allochthonous organic matter (OM) (including primary/reworked vitrinite and inertinite macerals) representing high influence by continental sediments (e.g., deltaic and littoral depositional environment) and (ii) rocks with dominant autochthonous OM (fluorescing liptinites such as alginite and their degraded remains) indicating more distal, productive marine continental shelf depositional environment. The latter is of main interest to this study as it is the only rock type that has the capability to generate oil while the former has very little contribution to oil generation potential due to the abundance of hydrogen-poor organic matter. The secondary maceral, solid bitumen, occurs within the mature section in the deeper part of the basin. Measured %VRo on vitrinite macerals ranges from 0.62 to 0.82% on four of the five wells studied indicating early oil window to oil window thermal maturity due to the mixing of the organic matter types mentioned above. Integrating Fluorescent Red/Green (R/G) quotient measurements from high intensity fluorescing alginite range from 0.77 to 0.86. Conversion of these values to %VRo equivalent range 0.58–0.66% indicates that thermal maturity has not yet reached the primary oil generation window. Vitrinite reflectance equivalent derived from solid bitumen (%BRo) in the deepest buried well ranges 1.10–1.16% indicating wet gas thermal maturity.

1. Introduction

Total organic carbon (TOC) content is one of the major parameters in source rock evaluation, however the ratio of labile to inert organic carbon and its thermal maturity generally control hydrocarbon potential of a source rock (Conford, 1998; Dembicki, 2009; Hackley et al., 2015; Synnott et al., 2017). Depositional environment and source of sediments are the major controlling factors of organic matter composition (e.g., Pratt, 1984; Bustin, 1988; Omura and Hoyanagi, 2004; Akande et al., 2012). Therefore, the estimation of allochthonous organic matter (including primary/reworked vitrinite and inertinite macerals) representing high influence by continental sediments (e.g., deltaic, littoral depositional environment) and autochthonous organic matter (fluorescing liptinites such as alginite and their degraded remains) helps to better understand the hydrocarbon potential of a source rock (e.g., Dewing and Sanei, 2009; Synnott et al., 2017; Yang and Horsfield, 2020).

Geochemical screening by programmed pyrolysis analysis such as Rock-Eval and HAWK TOC analyzer are often used for the assessment of source rock in conventional and unconventional hydrocarbon resource studies (Lafargue et al., 1998; Jarvie, 2012). The assessment of quantity, quality, and thermal maturity of organic matter by programmed

* Corresponding author. Husky Energy, 707 8th Avenue SW Calgary, AB T2P 3G7, Canada.
E-mail address: john.gordon1@ucalgary.ca (J.B. Gordon).

https://doi.org/10.1016/j.marpetgeo.2021.104965
Received 29 November 2020; Received in revised form 4 February 2021; Accepted 5 February 2021
Available online 17 February 2021

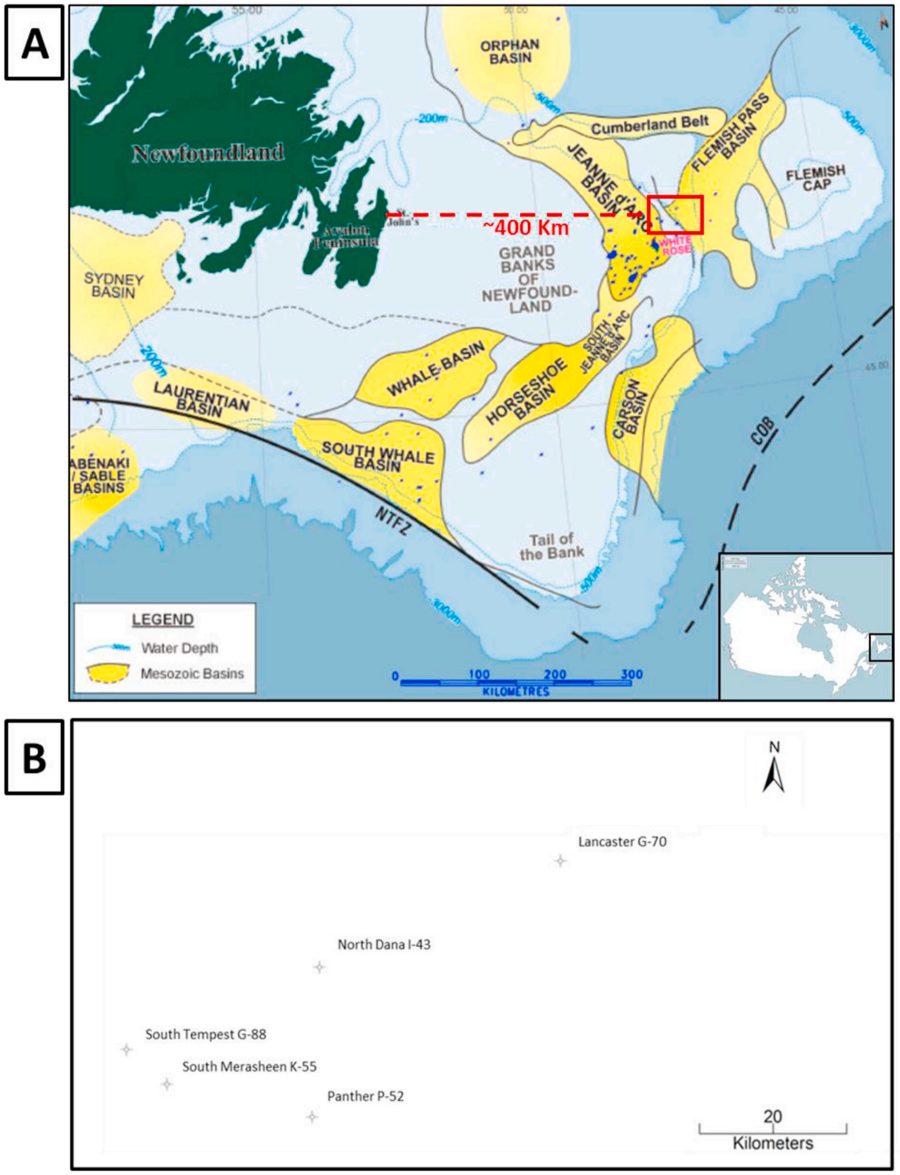

Fig. 1. A) A) Map showing the network of east coast Mesozoic basins (Modified from JWEL, 2001). Redbox shows the location of the five central ridge wells studied. Blue dots show well locations. B) Map showing a closer view of the locations and distribution of the five wells in this study area. (For interpretation of the references to color in this figure legend, the reader is referred to the Web version of this article.)

pyrolysis helps to better understand source rock hydrocarbon generation, retention and expulsion (Peters and Cassa, 1994; Carvajal-Ortiz and Gentzis, 2015; Yang and Horsfield, 2020). Although programmed pyrolysis is a great screening tool for estimating organic matter content, quality, and thermal maturity, additional analytical methods need to be used for an accurate source rock study (Carvajal-Ortiz and Gentzis, 2015; Yang and Horsfield, 2020). In addition, sample type for programmed pyrolysis analysis may compromise the measured parameters. Cutting samples are generally more susceptible to mud additive and up hole caving contamination than samples taken from drill core or sidewall cores (Sanei et al., 2020).

The Central Ridge area offshore Newfoundland, Canada (Fig. 1A and B) is a current targeted area for hydrocarbon exploitation (mainly oil production) from Upper Jurassic to Lower Cretaceous synrift sandstones with excellent reservoir quality in conventionally produced wells (Lowe et al., 2011). The Kimmeridgian-aged Egret Member of the Rankin Formation (Fig. 2) is considered the principle source rock in the neighboring Jeanne d' Arc basin (Swift and Williams, 1980; Creaney and Allison, 1987; Fowler et al., 1990, 1991; Huang et al., 1994; Fowler and McAlpine, 1995; DeSilva, 1999; Enachescu et al., 2010, 2012). It is also thought to be the equivalent source rock in the Central Ridge area (Fowler et al., 2007).

The Egret member, and the Central Ridge source rock equivalent, was deposited in a suboxic to anoxic, semi-silled marine environment, produced by rift tectonics during Oxfordian and Kimmeridgian time (von der Dick, 1989; Magoon et al., 2005) and was first described as a high hydrocarbon potential source rock (Swift and Williams, 1980). In contrast, other organic-rich mudrocks present in this area were deposited in a deltaic environment containing allochthonous continental degraded and reworked organic matter that is considered to have very low hydrocarbon generation potential. Previous studies on hydrocarbon potential of this basin have produced a plethora of publicly available programmed pyrolysis and vitrinite reflectance (VRo) data mainly using drill cutting samples. However, the main challenge in the interpretation of these datasets is in understanding the large standard deviation in the data caused by autochthonous organic matter along with the mixing of degraded allochthonous organic matter resulting in a wide range of organic matter types and thermal maturity that can render these

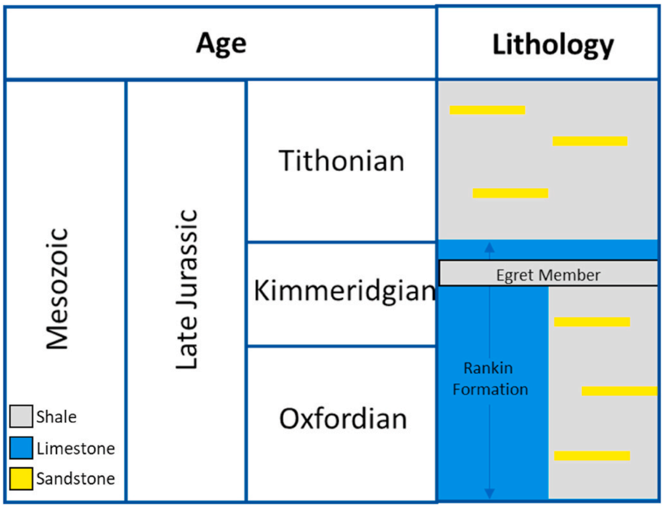

Fig. 2. Jeanne d' Arc lithostratigraphic chart showing the Tithonian and Kimmeridgian intervals of interest. The Rankin Formation and the Egret member are highlighted (Modified from Enachescu, 2005).

datasets unreliable and misleading.

In this study we re-examine the hydrocarbon potential from drill cuttings samples from the Kimmeridgian-aged source rock intervals and include Tithonian-aged source rock intervals from five Central Ridge wells using an integrated pyrolysis organic geochemistry and advanced organic petrology approach. The objective of this study is to re-investigate the thermal maturity, kerogen type and distribution, hydrocarbon potential, and depositional setting of the source rock intervals. It is the integration of these analytical techniques that provide insights to the identification and classification of the organic matter measured in programmed pyrolysis and vitrinite reflectance data. This leads to a better understanding of the distribution and the processes that affect the accumulation and preservation of source rocks in the Central ridge area. This provides ultimate value in the evaluation and mapping of source rock hydrocarbon potential in any global sedimentary basin (e.g., Passey et al., 2010; Gentzis et al., 2017).

2. Geological history

Prolific oil producing reservoirs can be found on the offshore eastern continental margin of Canada in numerous sedimentary basins that developed in response to different episodes of rifting events that took place from the Late Triassic to the Paleocene (Creaney and Allison, 1987). The Flemish Pass sub-basin formed during Late Triassic-Early Jurassic on the continental passive margin of the Grand Banks (Xiong et al., 2015). The basin is separated from the well-known Jeanne d'Arc Basin to the southwest by the Central Ridge (Foster and Robinson, 1993). Fig. 1A shows several sub basins in the offshore eastern continental margin of Canada and the approximate locations of Jeanne d'Arc Basin, Flemish Pass Basin and the Central Ridge. Sedimentological observations in several cored intervals in the neighboring Jeanne d' Arc Basin demonstrate a Jurassic/Cretaceous clastic shelf environment. The depositional environment is interpreted to be delta front to pro-delta facies with lateral variations to wave dominated shoreface deposits (BeicipFranlab, 2015). These depositional environments are believed to be similar in the Central Ridge area (BeicipFranlab, 2015).

The five wells selected for this study are located in the Central Ridge area approximately 420 km east of Sohn's Newfoundland in the Flemish Pass sub-basin (Fig. 1A and B). These conventionally drilled wells were originally drilled between 1980 and 1988 to explore for hydrocarbon accumulations in the Jurassic and Cretaceous-aged sandstone intervals. Analysis of the wells indicated insufficient oil producing potential and the wells were all abandoned (Cotterill, 1987, unpublished). Table 1 shows a brief history of each well according to the Canadian Newfoundland and Labrador Offshore Petroleum Board (C-NLOPB). The five wells were drilled through the Jurassic-aged Tithonian and Kimmeridgian source rock intervals that are the interest of this study (Fig. 2).

3. Sampling and methodology

All samples in this study were taken from drill cuttings. A general distrust of drill cuttings samples exists due to the nature of the sample collection methods assuming sample contamination by drilling mud additives and cavings from up hole formations (Sanei et al., 2020). The received cutting samples were washed in a light detergent solution, in an attempt to remove drilling fluid contamination. The cleaned samples were sieved to 1–2 mm size and hand-sorted/picked using tweezers under a binocular microscope. Only mudrock lithologies were selected from the drill cuttings samples for programmed pyrolysis analysis and reflectance measurements.

3.1. Programmed pyrolysis analysis

A total of one hundred and twenty-one samples were analyzed for hydrocarbon potential using programmed pyrolysis. Five drill cuttings samples from the Lancaster G-70 well representing the Early Tithonian (n = 4) and the Kimmeridgian (n = 1) intervals were sent to Schlumberger Reservoir Laboratory in Calgary, Alberta, Canada, for the standard cycle of a Vinci Technologies Rock Eval 6® analysis. Twenty-six drill cuttings samples from the Panther P-52 well representing the Kimmeridgian interval were sent to the Lithospheric Organic Carbon (LOC) laboratory, Department of Geoscience, Aarhus University in Denmark, for HAWK pyrolysis analysis. The remainder of the drill cuttings samples representing the Tithonian (n = 63) and Kimmeridgian (n = 27) intervals were sent to Wildcat Technologies in Humble Texas, USA, for HAWK pyrolysis analysis. A similar method was used for both HAWK and Rock Eval 6® analysis. The samples were finely ground and inserted into the analyzer. The pyrolysis method was carried out as described by Lafargue et al. (1998). The samples are held at an iso-temperature of 300 °C for 3 min. The temperature is then increased

Table 1
Summary of well history. All data from C-NLOPB website (https://www.cnlopb.ca/wells/).

Well	Spud Date	Reservoirs	Source Rock	Shows	Tests
North Dana I-43	1982	Jurassic sand units	345m Kimmeridgian		361606 M3/d gas 46.4 M3/d condensate
Panther P-52	1985	Jurassic sand units	519m Kimmeridgian	Minor in Kimmeridgian	None
South Tempest G-88	1980	Jurassic sand units	240m Kimmeridgian		150463 M3/d gas 268 M3/d oil
South Merasheen K-55	1988	Jurassic sand units	320m Kimmeridgian	Minor	0.8 M3/d gas 22 L oil
Lancaster G-70	1986	Jurassic sand units	674m Kimmeridgian	None	None

Table 2
Pyrolysis data.

Well ID	Stratigraphy	Depth m	Drilling Fluid	TOC wt.%	S1 mg HC/g
North Dana I-43	Early Tithonian	4115	Water-Based Mud	2.53	3.83
North Dana I-43	Early Tithonian	4155	Water-Based Mud	2.72	5.09
North Dana I-43	Early Tithonian	4195	Water-Based Mud	2.92	5.31
North Dana I-43	Early Tithonian	4235	Water-Based Mud	2.85	4.61
North Dana I-43	Early Tithonian	4275	Water-Based Mud	3.28	5.46
North Dana I-43	Early Tithonian	4315	Water-Based Mud	3.88	7.15
North Dana I-43	Early Tithonian	4355	Water-Based Mud	2.66	4.21
North Dana I-43	Early Tithonian	4375	Water-Based Mud	1.78	2.24
North Dana I-43	Early Tithonian	4395	Water-Based Mud	3.86	7.42
North Dana I-43	Early Tithonian	4415	Water-Based Mud	4.25	7.95
North Dana I-43	Early Tithonian	4425	Water-Based Mud	3.43	6.38
North Dana I-43	Early Tithonian	4475	Water-Based Mud	1.11	1.04
North Dana I-43	Early Tithonian	4485	Water-Based Mud	2.68	3.78
North Dana I-43	Early Tithonian	4565	Water-Based Mud	1.64	1.75
North Dana I-43	Early Tithonian	4625	Water-Based Mud	1.50	1.34
North Dana I-43	Early Tithonian	4665	Water-Based Mud	2.19	2.68
North Dana I-43	Early Tithonian	4705	Water-Based Mud	3.25	3.10
North Dana I-43	Kimmeridgian	4725	Water-Based Mud	1.18	0.80
North Dana I-43	Kimmeridgian	4745	Water-Based Mud	3.44	3.73
North Dana I-43	Kimmeridgian	4765	Water-Based Mud	3.39	8.10
North Dana I-43	Kimmeridgian	4785	Water-Based Mud	3.84	3.45
North Dana I-43	Kimmeridgian	4805	Water-Based Mud	2.97	2.12
North Dana I-43	Kimmeridgian	4825	Water-Based Mud	4.10	2.56
North Dana I-43	Kimmeridgian	5035	Water-Based Mud	2.96	1.61
North Dana I-43	Kimmeridgian	5055	Water-Based Mud	1.82	0.81
North Dana I-43	Kimmeridgian	5075	Water-Based Mud	2.67	1.41
Panther P-52	Early Tithonian	3230	Water-Based Mud	1.22	0.29
Panther P-52	Early Tithonian	3260	Water-Based Mud	1.54	0.55
Panther P-52	Early Tithonian	3305	Water-Based Mud	2.86	1.46
Panther P-52	Early Tithonian	3345	Water-Based Mud	4.01	2.16
Panther P-52	Early Tithonian	3380	Water-Based Mud	3.81	1.71
Panther P-52	Early Tithonian	3425	Water-Based Mud	1.71	0.73
Panther P-52	Early Tithonian	3465	Water-Based Mud	3.29	1.95
Panther P-52	Early Tithonian	3495	Water-Based Mud	2.74	1.37
Panther P-52	Early Tithonian	3525	Water-Based Mud	3.03	1.58
Panther P-52	Early Tithonian	3545	Water-Based Mud	4.28	2.86
Panther P-52	Early Tithonian	3565	Water-Based Mud	8.18	4.42
Panther P-52	Kimmeridgian	3755	Water-Based Mud	1.32	0.71
Panther P-52	Kimmeridgian	3760	Water-Based Mud	1.30	0.59
Panther P-52	Kimmeridgian	3775	Water-Based Mud	1.10	0.56
Panther P-52	Kimmeridgian	3780	Water-Based Mud	3.95	1.42
Panther P-52	Kimmeridgian	3790	Water-Based Mud	1.47	0.67
Panther P-52	Kimmeridgian	3805	Water-Based Mud	4.68	2.21
Panther P-52	Kimmeridgian	3815	Water-Based Mud	4.97	2.17
Panther P-52	Kimmeridgian	3825	Water-Based Mud	8.62	4.30
Panther P-52	Kimmeridgian	3830	Water-Based Mud	4.14	2.02
Panther P-52	Kimmeridgian	3840	Water-Based Mud	3.88	2.46
Panther P-52	Kimmeridgian	3855	Water-Based Mud	3.31	1.79
Panther P-52	Kimmeridgian	3860	Water-Based Mud	5.61	3.16
Panther P-52	Kimmeridgian	3870	Water-Based Mud	3.25	2.01
Panther P-52	Kimmeridgian	3885	Water-Based Mud	5.08	3.38
Panther P-52	Kimmeridgian	3890	Water-Based Mud	3.32	2.23
Panther P-52	Kimmeridgian	3905	Water-Based Mud	3.36	2.45
Panther P-52	Kimmeridgian	3915	Water-Based Mud	4.71	3.86
Panther P-52	Kimmeridgian	3945	Water-Based Mud	1.83	1.50
Panther P-52	Kimmeridgian	3950	Water-Based Mud	2.39	1.90
Panther P-52	Kimmeridgian	3965	Water-Based Mud	1.85	1.26
Panther P-52	Kimmeridgian	3975	Water-Based Mud	1.64	1.24
Panther P-52	Kimmeridgian	3980	Water-Based Mud	1.67	1.25
Panther P-52	Kimmeridgian	3995	Water-Based Mud	2.10	1.69
Panther P-52	Kimmeridgian	4005	Water-Based Mud	2.77	1.66
Panther P-52	Kimmeridgian	4014	Water-Based Mud	1.31	1.03
Panther P-52	Kimmeridgian	4025	Water-Based Mud	0.97	0.56
South Tempest G-88	Late Tithonian	3470	Water-Based Mud	0.82	0.15
South Tempest G-88	Late Tithonian	3505	Water-Based Mud	0.99	0.18
South Tempest G-88	Late Tithonian	3515	Water-Based Mud	0.95	0.17
South Tempest G-88	Late Tithonian	3555	Water-Based Mud	1.06	0.11
South Tempest G-88	Late Tithonian	3565	Water-Based Mud	0.99	0.18
South Tempest G-88	Late Tithonian	3645	Water-Based Mud	1.16	0.35
South Tempest G-88	Late Tithonian	3655	Water-Based Mud	1.15	0.37
South Tempest G-88	Late Tithonian	3665	Water-Based Mud	0.87	0.20
South Tempest G-88	Early Tithonian	3745	Water-Based Mud	3.68	3.72
South Tempest G-88	Early Tithonian	3765	Water-Based Mud	2.16	2.04
South Tempest G-88	Early Tithonian	3785	Water-Based Mud	2.17	1.80

(*continued on next page*)

Table 2 (*continued*)

Well ID	Stratigraphy	Depth m	Drilling Fluid	TOC wt.%	S1 mg HC/g
South Tempest G-88	Early Tithonian	3805	Water-Based Mud	2.91	3.11
South Merasheen K-55	Late Tithonian	2435	Oil-Based Mud	1.73	0.07
South Merasheen K-55	Late Tithonian	2445	Oil-Based Mud	1.78	0.08
South Merasheen K-55	Late Tithonian	2475	Oil-Based Mud	2.50	0.11
South Merasheen K-55	Late Tithonian	2495	Oil-Based Mud	4.31	0.17
South Merasheen K-55	Late Tithonian	2505	Oil-Based Mud	6.61	0.26
South Merasheen K-55	Early Tithonian	2545	Oil-Based Mud	2.06	0.08
South Merasheen K-55	Early Tithonian	2555	Oil-Based Mud	3.24	0.10
South Merasheen K-55	Early Tithonian	2595	Oil-Based Mud	2.95	0.10
South Merasheen K-55	Early Tithonian	2635	Oil-Based Mud	3.02	0.11
South Merasheen K-55	Early Tithonian	2645	Oil-Based Mud	3.43	0.14
South Merasheen K-55	Early Tithonian	2655	Oil-Based Mud	4.34	0.16
South Merasheen K-55	Early Tithonian	2665	Oil-Based Mud	3.99	0.18
South Merasheen K-55	Early Tithonian	2675	Oil-Based Mud	4.46	0.21
South Merasheen K-55	Early Tithonian	2685	Oil-Based Mud	1.44	0.07
South Merasheen K-55	Early Tithonian	2715	Oil-Based Mud	3.09	0.15
South Merasheen K-55	Early Tithonian	2725	Oil-Based Mud	1.85	0.09
South Merasheen K-55	Early Tithonian	2745	Oil-Based Mud	1.27	0.09
South Merasheen K-55	Early Tithonian	2765	Oil-Based Mud	1.61	0.11
South Merasheen K-55	Early Tithonian	2775	Oil-Based Mud	1.55	0.10
South Merasheen K-55	Early Tithonian	2785	Oil-Based Mud	0.91	0.07
South Merasheen K-55	Early Tithonian	2795	Oil-Based Mud	2.45	0.13
South Merasheen K-55	Early Tithonian	2815	Oil-Based Mud	1.53	0.09
South Merasheen K-55	Early Tithonian	2830	Oil-Based Mud	0.60	0.05
South Merasheen K-55	Kimmeridgian	3015	Oil-Based Mud	1.26	0.09
South Merasheen K-55	Kimmeridgian	3035	Oil-Based Mud	1.38	0.09
South Merasheen K-55	Kimmeridgian	3055	Oil-Based Mud	1.45	0.08
South Merasheen K-55	Kimmeridgian	3075	Oil-Based Mud	3.30	0.13
South Merasheen K-55	Kimmeridgian	3095	Oil-Based Mud	2.16	0.10
South Merasheen K-55	Kimmeridgian	3115	Oil-Based Mud	2.09	0.10
South Merasheen K-55	Kimmeridgian	3135	Oil-Based Mud	3.58	0.15
South Merasheen K-55	Kimmeridgian	3155	Oil-Based Mud	2.20	0.11
South Merasheen K-55	Kimmeridgian	3175	Oil-Based Mud	2.60	0.10
South Merasheen K-55	Kimmeridgian	3205	Oil-Based Mud	3.52	0.14
South Merasheen K-55	Kimmeridgian	3225	Oil-Based Mud	1.64	0.10
South Merasheen K-55	Kimmeridgian	3245	Oil-Based Mud	4.18	0.14
South Merasheen K-55	Kimmeridgian	3315	Oil-Based Mud	1.73	0.10
South Merasheen K-55	Kimmeridgian	3335	Oil-Based Mud	2.96	0.14
South Merasheen K-55	Kimmeridgian	3355	Oil-Based Mud	1.93	0.11
South Merasheen K-55	Kimmeridgian	3375	Oil-Based Mud	2.20	0.12
South Merasheen K-55	Kimmeridgian	3395	Oil-Based Mud	0.89	0.07
South Merasheen K-55	Kimmeridgian	3425	Oil-Based Mud	1.04	0.08
Lancaster G-70	Early Tithonian	3300	Water-Based Mud	2.24	0.37
Lancaster G-70	Early Tithonian	3440	Water-Based Mud	1.96	0.46
Lancaster G-70	Early Tithonian	3580	Water-Based Mud	3.08	3.20
Lancaster G-70	Early Tithonian	3620	Water-Based Mud	2.99	3.63
Lancaster G-70	Kimmeridgian	3680	Water-Based Mud	3.81	3.39

S2 mg HC/g	S3 mg CO2/g	Tmax °C	HI S2x100/TOC	OI S3x100/TOC	PI (S1/(S1+S2))
4.17	0.55	447	164	21	0.48
4.51	0.62	446	166	22	0.53
4.09	0.60	447	140	20	0.56
3.86	0.65	450	135	22	0.54
4.02	0.73	450	122	22	0.58
4.82	1.00	451	124	25	0.60
2.83	0.85	453	106	32	0.60
1.36	5.40	440	76	303	0.62
4.74	1.82	435	122	47	0.61
5.43	0.98	457	127	23	0.59
3.85	0.72	456	112	20	0.62
0.79	0.49	453	70	43	0.57
2.29	0.85	439	85	31	0.62
1.43	1.10	450	87	67	0.55
0.95	0.72	454	63	47	0.59
2.41	1.28	403	110	58	0.53
1.87	0.89	455	57	27	0.62
0.51	0.88	433	43	74	0.61
1.71	1.68	420	49	48	0.69
4.28	3.24	319	126	95	0.65
2.05	2.39	422	53	62	0.63
1.70	0.78	468	57	26	0.55
2.34	1.27	445	57	30	0.52
1.02	0.94	476	34	31	0.61
0.59	0.60	471	32	33	0.58

(*continued on next page*)

Table 2 (*continued*)

S2 mg HC/g	S3 mg CO2/g	Tmax °C	HI S2x100/TOC	OI S3x100/TOC	PI (S1/(S1+S2))
1.08	1.01	454	40	37	0.57
2.32	0.43	438	190	35	0.11
7.47	0.32	432	484	20	0.07
16.32	0.56	427	570	19	0.08
24.97	0.59	428	622	14	0.08
23.72	0.57	435	622	15	0.07
6.10	0.49	440	357	28	0.11
16.82	0.48	434	511	14	0.10
13.62	0.68	430	497	24	0.09
15.37	0.51	433	507	16	0.09
25.65	0.42	432	599	9	0.10
54.15	0.54	434	661	6	0.08
2.37	1.17	435	180	88	0.23
1.59	1.67	434	122	128	0.27
1.13	1.41	436	102	128	0.33
13.86	0.79	424	350	20	0.09
2.17	1.37	437	147	92	0.24
20.90	0.89	432	446	19	0.10
19.93	0.70	436	401	14	0.10
44.00	0.67	431	510	7	0.09
18.86	0.54	437	455	13	0.10
13.87	0.71	438	357	18	0.15
12.01	0.64	438	362	19	0.13
24.47	0.79	437	435	14	0.11
9.54	0.56	438	293	17	0.17
19.16	0.60	438	377	11	0.15
9.66	0.70	439	290	21	0.19
10.59	0.75	438	315	22	0.19
11.89	0.97	441	252	20	0.25
3.89	0.89	441	212	48	0.28
6.01	0.78	438	251	32	0.24
3.62	1.23	440	195	66	0.26
3.08	1.45	440	188	88	0.29
3.10	1.40	440	185	83	0.29
5.09	0.77	440	243	36	0.25
5.94	0.92	440	214	33	0.22
2.45	1.08	439	187	82	0.30
1.17	1.06	441	121	109	0.32
0.65	0.41	438	79	49	0.19
0.75	0.60	441	75	60	0.19
0.83	0.52	438	87	54	0.17
0.52	0.47	441	48	44	0.17
0.70	0.54	442	70	54	0.20
1.23	0.49	439	106	42	0.22
0.90	0.63	444	78	54	0.29
0.63	0.79	443	72	91	0.24
13.57	0.52	435	369	14	0.22
5.83	0.34	444	269	15	0.26
6.36	0.46	444	292	20	0.22
9.40	0.39	443	323	13	0.25
3.20	0.34	434	185	19	0.02
4.04	0.41	431	227	22	0.02
11.74	0.39	427	468	15	0.01
30.00	0.52	422	695	12	0.01
48.87	0.51	420	739	7	0.01
7.57	0.37	428	366	18	0.01
13.40	0.39	428	413	12	0.01
14.53	0.48	425	493	16	0.01
14.49	0.38	425	479	12	0.01
19.22	0.48	419	560	13	0.01
29.08	0.50	418	670	11	0.01
24.88	0.40	418	622	10	0.01
30.13	0.46	421	675	10	0.01
2.91	0.41	427	202	28	0.02
15.70	0.60	426	508	19	0.01
6.40	0.30	426	345	16	0.01
1.88	0.45	430	147	35	0.05
4.35	0.38	427	271	23	0.02
5.63	0.38	427	363	24	0.02
0.83	0.34	433	90	37	0.08
6.10	0.61	430	249	24	0.02
1.39	0.50	435	90	32	0.06
0.27	0.39	431	45	65	0.16
4.44	0.28	426	352	22	0.02
6.30	0.31	426	457	22	0.01

(*continued on next page*)

Table 2 (*continued*)

S2 mg HC/g	S3 mg CO2/g	Tmax °C	HI S2x100/TOC	OI S3x100/TOC	PI (S1/(S1+S2))
6.26	0.30	427	431	20	0.01
20.68	0.32	427	626	9	0.01
11.33	0.41	427	524	19	0.01
7.98	0.28	426	382	13	0.01
20.48	0.36	426	571	10	0.01
11.93	0.18	427	542	8	0.01
14.56	0.32	428	559	12	0.01
23.39	0.44	426	664	12	0.01
6.31	0.31	429	384	19	0.02
28.13	0.31	427	672	7	0.00
6.83	0.35	431	393	20	0.01
17.37	0.34	433	587	11	0.01
8.57	0.26	443	443	13	0.01
10.80	0.28	442	491	12	0.01
1.15	0.32	445	128	35	0.06
0.76	0.34	442	73	32	0.10
4.17	0.98	422	144	44	0.08
2.84	1.28	428	145	65	0.14
5.58	1.27	427	181	41	0.36
5.60	1.23	427	187	41	0.39
18.89	1.29	421	496	34	0.15

at 25 °C per minute until a final temperature of 650 °C is achieved. The output pyrogram S1 and S2 (mg HC/g) peaks correspond to the free hydrocarbon and thermally cracked kerogen, respectively. The concentration of CO_2 released during pyrolysis corresponds to the S3, representing the oxygen containing carbon in the kerogen. Further oxidation heating of the sample to 850 °C incinerates the residual organic carbon and is calculated as total organic carbon (TOC) of the sample (Lafargue et al., 1998).

3.2. Organic petrology

Twenty-eight samples were selected for organic petrology representing large variations in the pyrolysis data. The samples were prepared into epoxy-resin sample pellets. The pellets were finely polished to remove any irregularities on the surface of the pellet. Petrographic analysis was completed on a Zeiss Axio Imager II microscope equipped with the Diskus-Fossil system for the full range of photometry (reflectance measurements), fluorescence spectrometry and multigrid maceral distribution analysis at the LOC laboratory in the Department of Geoscience, Aarhus University and the Geological Survey of Canada, Calgary. An ultrafine measurement probe (0.3 μm^2 spot size) was used for random reflectance measurements under oil immersion (refractive index, n = 1.518 at 23 °C). An yttrium-aluminum-garnet reference standard was used with a reflectance of 0.906% under oil immersion. The entire surface of the pellet was examined at 50× magnification to obtain the measurements. Fluorescence properties were also measured on eight drill cutting samples, using the Hilgers Fluo Mode to measure the red to green ratio. Instead of measuring the full spectrum in the visible light range (400–700 nm), this method uses two filter cubes to measure intensity of fluorescence at 600 nm (red cube) and 520–570 nm (green cube) and is fully comparable with fluorescence spectrometry. The difference is this method provides point measurements at only two, red and green, wavelengths using the following specifications (Hilgers Technisches Buero):

Red-Cube:
Excitation Filter BP 450-490.
Beam splitter LP 515.
Emission Filter DT Red Linos LP600.
Green-Cube:
Excitation Filter BP 450-490.
Beam splitter LP 515.
Emission Filter DT Green Linos BP520-570.

A novel twenty-one cross-hair grid for point counting organic macerals was applied. A grid consisting of twenty-one points is applied to the microscope field of view combined with a motorized automated microscope stage. This allows for the scanning of the surface of each polished pellet in equal intervals. Organic macerals were counted when intercepted by any of the twenty-one crosses in each frame. The samples were scanned under a 50× oil immersion objective with a maximum of 100 × 100 frames per sample. Two hundred maceral counts per sample were counted for maceral distribution analysis and care was taken to only count areas within the rock matrix and avoid organic fragments which appear isolated in the sample binder. Four groups of macerals (vitrinite, inertinite, liptinite, and solid bitumen) were determined based on the macerals physical attributes as described in ICCP (1994).

4. Results and discussion

4.1. Programed pyrolysis and organic geochemistry

The collected programmed pyrolysis data and the organic petrology data are presented in Tables 2 and 3, respectively. The total organic carbon (TOC) content values from all the samples collected (n = 121) range from 0.60 to 8.62 (wt. %). S2 values range from 0.27 to 54.15 (mg HC/g). The hydrogen index (HI) and oxygen index (OI) values range from 32 to 739 (mg HC/g TOC) and 6 to 303 (mg CO2/g TOC), respectively. Tmax values range from 319 to 476 °C. Tmax values less than 400 °C are considered instrument artifacts as the instrument cannot find a substantial S2 peak in the FID signal (Peters, 1986; Peters and Cassa, 1994). Therefore, Tmax values less than 400 °C and were culled from the data interpretations. The composite depth profiles of TOC, S2, HI, and OI are shown in Fig. 4. The deepest well, North Dana I-43 shows a clear decrease in hydrocarbon potential (S2 and HI) and TOC as compared to the samples from the other four wells in the study area. The range of values in the other four wells show a large variation with clear depth trend for all pyrolysis parameters within each well (Fig. 3).

The S2 versus TOC plot (Fig. 4a) shows the samples from all wells have good to excellent TOC content. However, their hydrocarbon potential (S2 mg HC/g) varies drastically from poor to excellent. The wide range of S2 is related to four factors (i) primary production of hydrogen-rich algal matter (ii) preservation of algal matter during and after deposition, (iii) dilution by the hydrogen-poor land-derived organic matter, and finally (iv) thermal maturity and hydrocarbon generation and expulsion (Conford, 1998; Synnott et al., 2017). The first three factors are related to the depositional environment and the fourth factor is related to burial depth.

Table 3
Organic petrology data collected on selected samples.

Sample Information

Well ID	Stratigraphy	Sample #	Depth m	Drilling Fluid
North Dana I-43	Early Tithonian	ND-01	4115	Water Based Mud
North Dana I-43	Early Tithonian	ND-02	4315	Water Based Mud
North Dana I-43	Early Tithonian	ND-03	4705	Water Based Mud
North Dana I-43	Kimmeridgian	ND-04	4745	Water Based Mud
North Dana I-43	Kimmeridgian	ND-05	4825	Water Based Mud
North Dana I-43	Kimmeridgian	ND-06	5075	Water Based Mud
South Tempest G-88	Late Tithonian	ST-01	3515	Water Based Mud
South Tempest G-88	Late Tithonian	ST-02	3645	Water Based Mud
South Tempest G-88	Early Tithonian	ST-03	3745	Water Based Mud
South Tempest G-88	Early Tithonian	ST-04	3805	Water Based Mud
Panther P-52	Early Tithonian	P-01	3230	Water Based Mud
Panther P-52	Early Tithonian	P-02	3260	Water Based Mud
Panther P-52	Early Tithonian	P-03	3305	Water Based Mud
Panther P-52	Early Tithonian	P-04	3425	Water Based Mud
Panther P-52	Early Tithonian	P-05	3465	Water Based Mud
Panther P-52	Early Tithonian	P-06	3565	Water Based Mud
Panther P-52	Kimmeridgian	P-08	3825	Water Based Mud
Panther P-52	Kimmeridgian	P-10	3905	Water Based Mud
Panther P-52	Kimmeridgian	P-12	4025	Water Based Mud
South Merasheen K-55	Late Tithonian	SM-01	2445	Oil Based Mud
South Merasheen K-55	Late Tithonian	SM-03	2505	Oil Based Mud
South Merasheen K-55	Early Tithonian	SM-04	2545	Oil Based Mud
South Merasheen K-55	Early Tithonian	SM-07	2675	Oil Based Mud
South Merasheen K-55	Kimmeridgian	SM-12	3225	Oil Based Mud
South Merasheen K-55	Kimmeridgian	SM-13	3245	Oil Based Mud
Lancaster G-70	Early Tithonian	LAN-15	3440	Water Based Mud
Lancaster G-70	Early Tithonian	LAN-20	3580	Water Based Mud
Lancaster G-70	Kimmeridgian	LAN-25	3680	Water Based Mud

Pyrolysis Data

TOC wt%	S1 mg HC/g	S2 mg HC/g	S3 mg CO2/g	Tmax °C	HI S2x100/TOC	OI S3x100/TOC	PI (S1/(S1+S2))
2.53	3.83	4.17	0.55	447	164	21	0.48
3.88	7.15	4.82	1.00	451	124	25	0.60
3.25	3.10	1.87	0.89	455	57	27	0.62
3.44	3.73	1.71	1.68	420	49	48	0.69
4.10	2.56	2.34	1.27	445	57	30	0.52
2.67	1.41	1.08	1.01	454	40	37	0.57
0.95	0.17	0.83	0.52	438	87	54	0.17
1.16	0.35	1.23	0.49	439	106	42	0.22
3.68	3.72	13.57	0.52	435	369	14	0.22
2.91	3.11	9.4	0.39	443	323	13	0.25
1.22	0.29	2.32	0.43	438	190	35	0.11
1.54	0.55	7.47	0.32	432	484	20	0.07
2.86	1.46	16.32	0.56	427	570	19	0.08
1.71	0.73	6.1	0.49	440	357	28	0.11
3.29	1.95	16.82	0.48	434	511	14	0.10
8.18	4.42	54.15	0.54	434	661	6	0.08
8.62	2.92	44	0.61	431	510	7	0.06
3.36	1.11	10.59	0.67	438	315	19	0.10
0.96	0.38	1.17	0.92	441	121	95	0.24
1.78	0.08	4.04	0.41	431	227	22	0.02
6.61	0.26	48.87	0.51	420	739	7	0.01
2.06	0.08	7.57	0.37	428	366	18	0.01
4.46	0.21	30.13	0.46	421	675	10	0.01
1.64	0.1	6.31	0.31	429	384	19	0.02
4.18	0.14	28.13	0.31	427	672	7	0.01
1.96	0.46	2.84	1.28	428	145	65	0.14
3.08	3.2	5.58	1.27	427	181	41	0.36
3.81	3.39	18.89	1.29	421	496	34	0.15

Maceral Point Count Data (Normalized to TOC)							Maceral Ternary Data		
Vitrinite %	Reworked Vitrinite %	Inertinite %	Liptinite %	Degraded Liptinite %	Solid Bitumen %	Total %	V + I %	B %	L %
	41		14	3	42	100	41	42	17
9	25	1	9	16	40	100	36	39	25
3	2		10		85	100	5	85	10
	18		16	2	64	100	18	64	18
12	7	4	6	7	64	100	30	57	13
	5		6		89	100	5	89	6
1	19		76	4		100	20		80
2	31		59	8		100	33		67

(*continued on next page*)

Table 3 (*continued*)

Maceral Point Count Data (Normalized to TOC)							Maceral Ternary Data		
Vitrinite %	Reworked Vitrinite %	Inertinite %	Liptinite %	Degraded Liptinite %	Solid Bitumen %	Total %	V + I %	B %	L %
1	10		83	6		100	11		89
5	33	2	19	38	3	100	40	3	57
5	45		40	9	1	100	50	1	49
1	10		86	3		100	11		89
7	10	10	60	12	1	100	27	1	72
8	26	1	61	4		100	35		65
4	7		88	1		100	11		89
2	8		84	6		100	10		90
	3		94	3		100	3		97
4	16	3	33	44		100	23		77
8	57	1	20	11	3	100	66	3	31
2	34		35	29		100	36		64
5	13		61	21		100	18		82
3	49		37	11		100	52		48
2	5	1	92	1		100	8		92
3	32		41	23	1	100	35	1	64
4	1		90	4	1	100	5	1	94
1	45		28	23	3	100	46	3	51
7	28		29	34	2	100	35	2	63
1	17	1	72	9		100	19		81

Vitrinite Reflectance and Fluorescence Data			
Calculated %Ro (0.0180 x Tmax) - 7.16	Measured %Ro	R/G Q λ_{max}	R/G Q Based on Inan et al. (2016)
0.89	1.10		
0.96	1.10		
1.03	1.14		
0.40	1.16		
0.85	1.12		
1.01	1.12		
0.72	0.76	0.84	0.60
0.74	0.77		
0.67	0.79		
0.81	0.79	0.86	0.61
0.72	0.72		
0.62	0.62		
0.53	0.72		
0.76	0.70		
0.65	0.66	0.78	0.58
0.65	0.67		
0.60	0.65	0.85	0.60
0.72	0.64	0.86	0.60
0.78	0.79		
0.60	0.74		
0.40	0.65	0.80	0.59
0.54	0.82		
0.42	0.70	0.77	0.58
0.56	0.74		
0.53	0.64	0.77	0.58
0.54	0.72		
0.53	0.72		
0.42	0.73	0.89	0.66

The pseudo van Krevelen plot (Fig. 4b) for all the samples shows the ranges for Type I oil prone organic matter, Type II oil prone, Type II/III mixed organic matter, and Type III gas prone organic matter. The samples from North Dana I-43 well plot relatively closer to the x (HI) and y (OI) axes compared to the other wells. This is the typical maturity trend for organic matter, irrespective of the organic matter types, in which hydrogen and oxygen are lost during the thermal maturity and residual carbon is enriched (Peters et al., 2015). This would lead to progressive depletion of HI and OI along the defined kerogen type lines in the pseudo van Krevelen diagram. In contrast, the samples from the other four wells demonstrate an inverse (HI = 1/OI) trend in the pseudo van Krevelen diagram. This relationship can be described as progressive depletion of HI associated with increase in OI and vice versa. This is quite distinct from the maturity trend which both HI and OI are depleted with maturity. The inverse HI = 1/OI trend is characteristic of the transitioning depositional environment from liptinitic rich aquatic environment with abundant production and excellent preservation of hydrogen-rich algal matter (marine, shallow marine) to the aquatic environment with influence or large input from the oxygen-rich terrigenous organic matter (littoral and/or deltaic environment) and vice versa (Omura and Hoyanagi, 2004; Hackley et al., 2020). The pseudo van Krevelen diagram for samples from the four wells (except North Dana I-43) show the transitioning oscillations between the restricted marine and deltaic environments (e.g., Pratt, 1984; Bustin, 1988; Akande et al., 1998; Omura and Hoyanagi, 2004).

The HI versus Tmax plot (Fig. 4c) shows the South Merasheen K-55 and Lancaster G-70 wells oscillating from Type II to Type III organic matter in the immature phase. The Panther P-52 and South Tempest K-55 wells range from early maturity to oil window. The North Dana I-43 well falls within end of oil window to gas window.

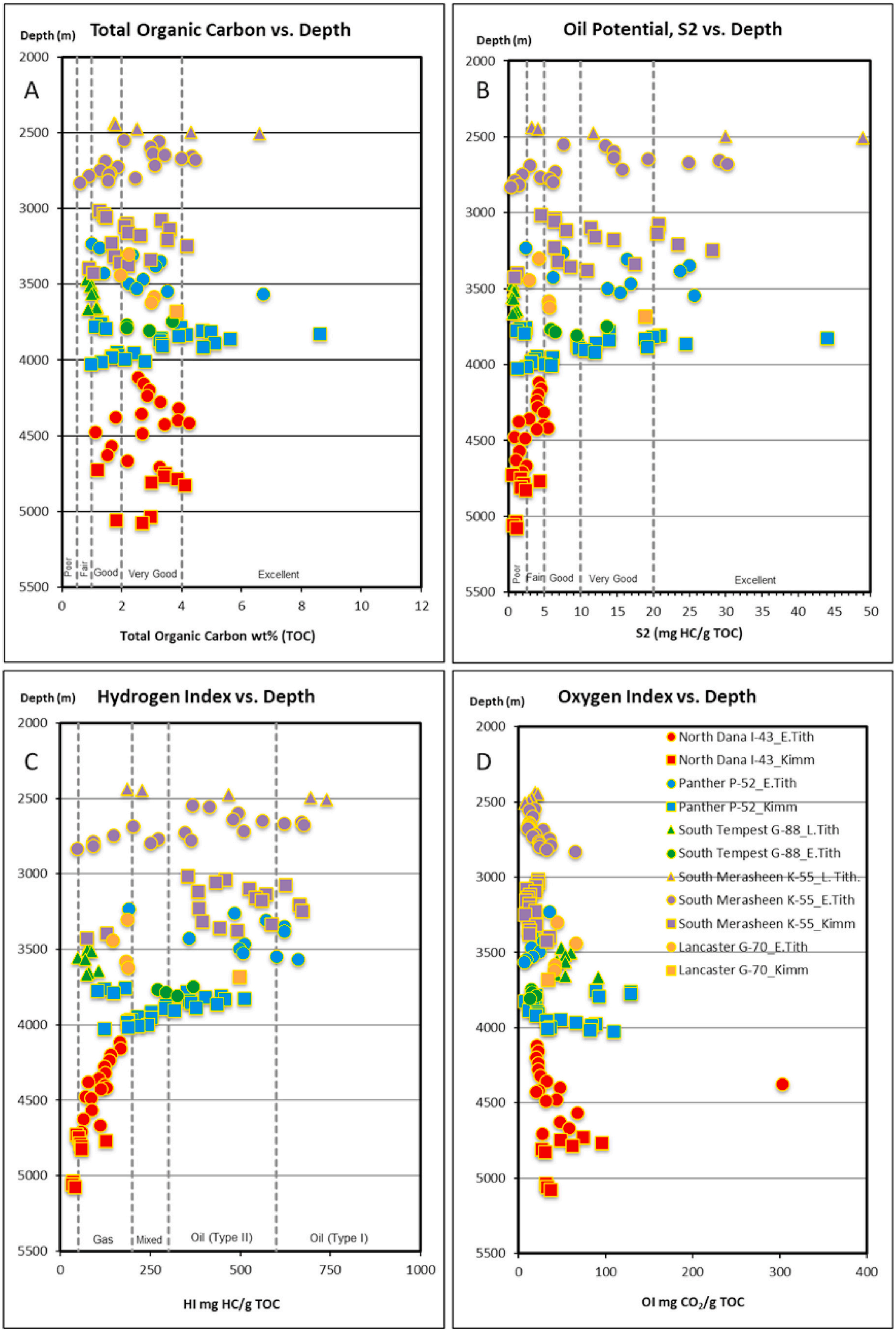

Fig. 3. HAWK pyrolysis data by depth. A) Total Organ Carbon by depth. B) Oil potential S2 by depth. C) Hydrogen Index by depth. D) Oxygen Index by depth.

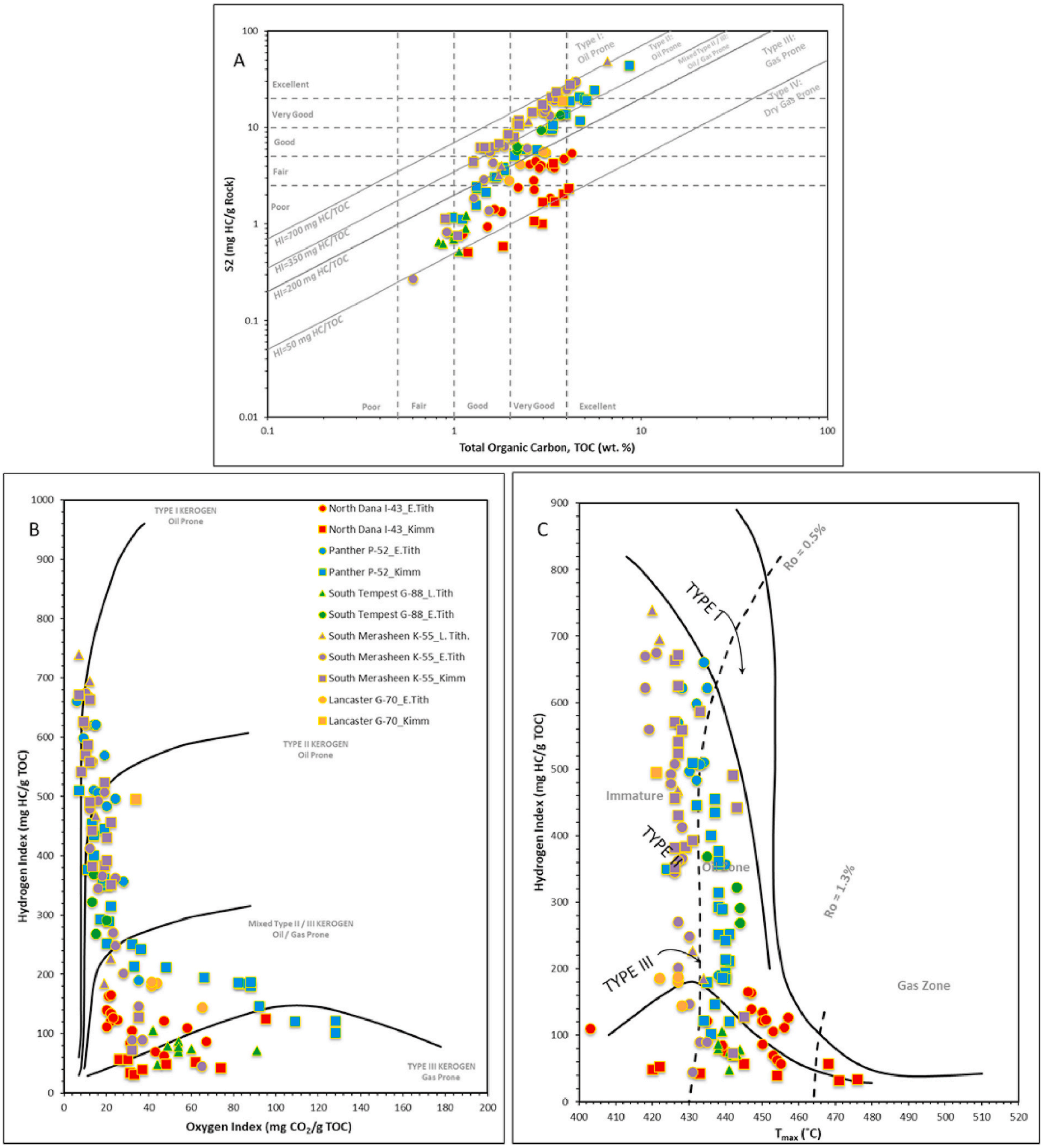

Fig. 4. HAWK pyrolysis data. A) S2 vs. Total organic carbon (TOC). B) Pseudo van Krevelen plot. C) Hydrogen Index (HI) vs. Tmax. These plots show the wide range of kerogen types, thermal maturity, and hydrocarbon potential present in the Tithonian and Kimmeridgian source rock intervals in the Central Ridge area.

4.2. Organic petrology

Point count data shows a wide variety of maceral types to be present in all the wells and age intervals including vitrinite (Type III) exhibiting a %VRo ranging 0.5–0.8%, high-reflecting reworked vitrinite (Type IV) that has a brighter grey colour than vitrinite and %VRo ranging 0.9–1.2%, liptinite (Type II), inertinite (Type IV) exhibiting bright grey color and high %VRo values (1.2–1.9%), and solid bitumen (mainly in-situ bituminized lamalginites; Table 2). Maceral point count data are normalized to measured TOC values. North Dana I-43 is the only well with abundant solid bitumen. Representative photomicrographs of the point counted maceral types are illustrated in Fig. 5A to 5L.

The OM composition can be divided into three main groups based on depositional environment (i) marine-derived liptinite-rich (oil-prone Type II), (ii) mixed Type II/III, and (iii) terrigenous-derived vitrinite-rich (Type III/IV). The OM preservation in these three groups is defined by oscillation in sea level from a marine influenced OM maceral composition to more terrigenous littoral and/or deltaic influenced OM composition. This depositional environment influence is represented by repeating cycles throughout the entire Kimmeridgian and Tithonian section regardless of burial depth or age of the sediment. South Merasheen K-55 and Lancaster G-70 wells are oscillating from bright yellow green fluorescing marine Type II lamalginite (Fig. 5A and B) to Type III vitrinite (Fig. 5C) with varying amounts of inertinite (Fig. 5D). The Panther P-52 samples contains bright yellow green fluorescing Type II lamalginites and fluorescing amorphous liptinite (Fig. 5E and F). Occurrence of exsudatinite observed in these samples suggests an early oil window maturity. Exsudatinite is a secondary, early generated

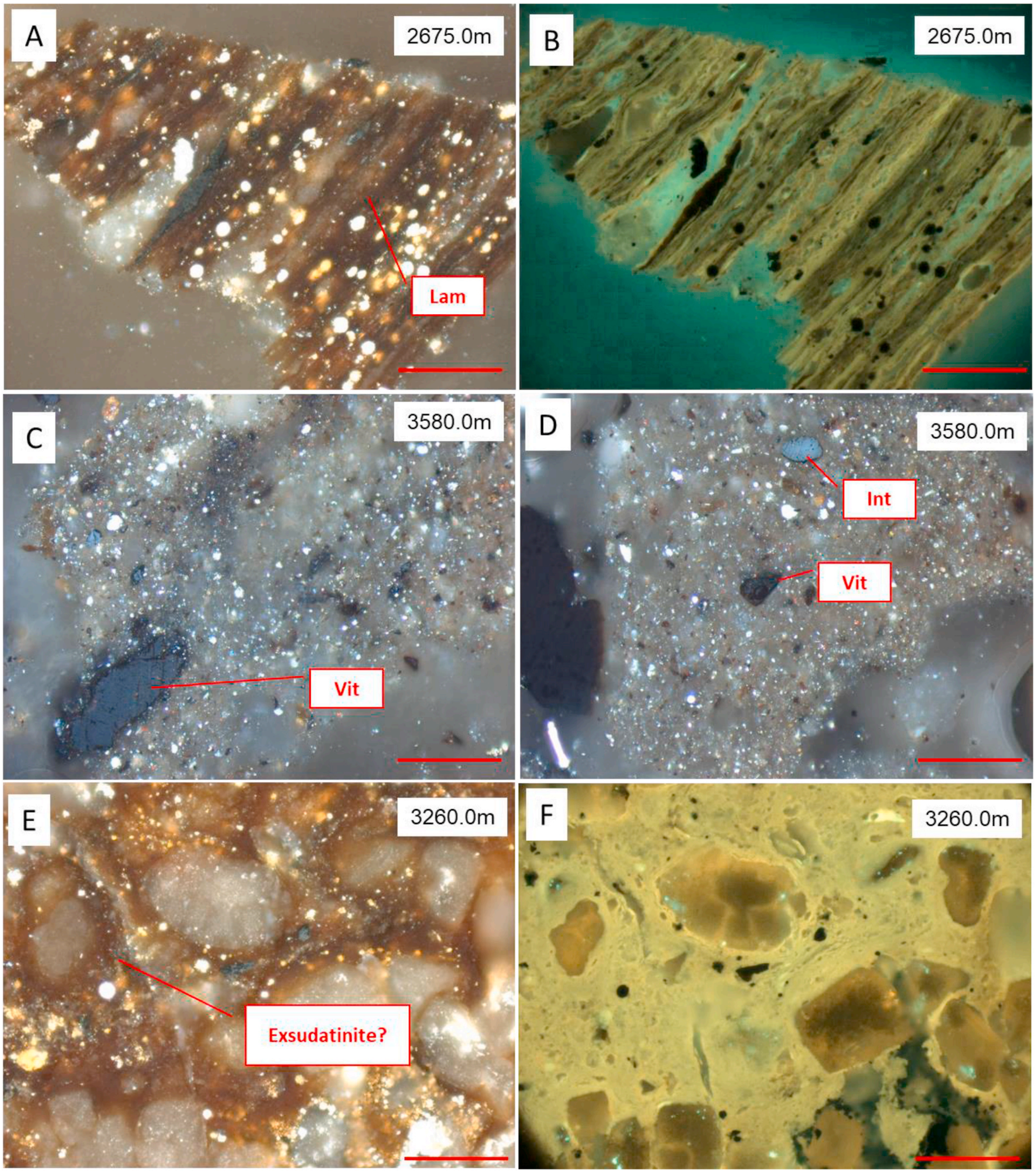

Fig. 5. Photomicrographs showing different types of organic particles. All photomicrographs are taken. under white light with oil immersion and a 50 × objective was used. Red scale bar is 50 μm in length.A) South Merasheen K-55. Dark brown layers of lamalginite (Lam) displaying thick layers. B) As in photo A but under fluorescence. C) Lancaster G-70. Vitrinite fragment (Vit) in a silty argillaceous matrix D) Lancaster G-70. Example of vitrinite (Vit) and inertinite (Int) in a silty argillaceous matrix. E) Panther P-52. Brown pore-filling liptinite (Exsudatinite?) in a carbonate matrix. F) As in photo E, but under fluorescence highlighting bright green fluorescence color. G) South Tempest G-88. Lamalginite (Lam) exhibiting bright yellow-red fluorescence suggesting the early oil window thermal maturity. Under fluorescence. H) South Tempest G-88. Fine layers of bright yellow-green algae composed of thin-walled colonial or unicellular algae that occur as distinct laminae. I) North Dana I-43. Solid bitumen (Bit) exhibiting flow structure. J) North Dana I-43. Large vitrinite (Vit) fragment. K) North Dana I-43. Assemblage of filamentous algae (Alg) that has been bituminized. L) North Dana I-43. A paired image showing bituminized alga under plain light (left) and under fluorescence light (right). Small algal fragments are fluorescing a dark brown color and large bituminized filamentous algae do not fluoresce at all suggesting a high degree of alteration. Note abundant pyrite. . (For interpretation of the references to color in this figure legend, the reader is referred to the Web version of this article.)

bitumen product expelled in oil shales that forms from seeping bitumen into open pore spaces (Teichmüller, 1973; Goodarzi et al., 2019). Exsudatinite is recognized as brownish (in white reflected light microscopy), often yellow fluorescing, viscous, amorphous matter (Sanei, 2020). The South Tempest G-88 samples shows similar OM composition to Panther P-52 (Fig. 5G). Fine layers of bright yellow green algae composed of thin-walled colonial or unicellular algae occur as distinct laminae (Fig. 5H). The fluorescence color of the lamalginite in these

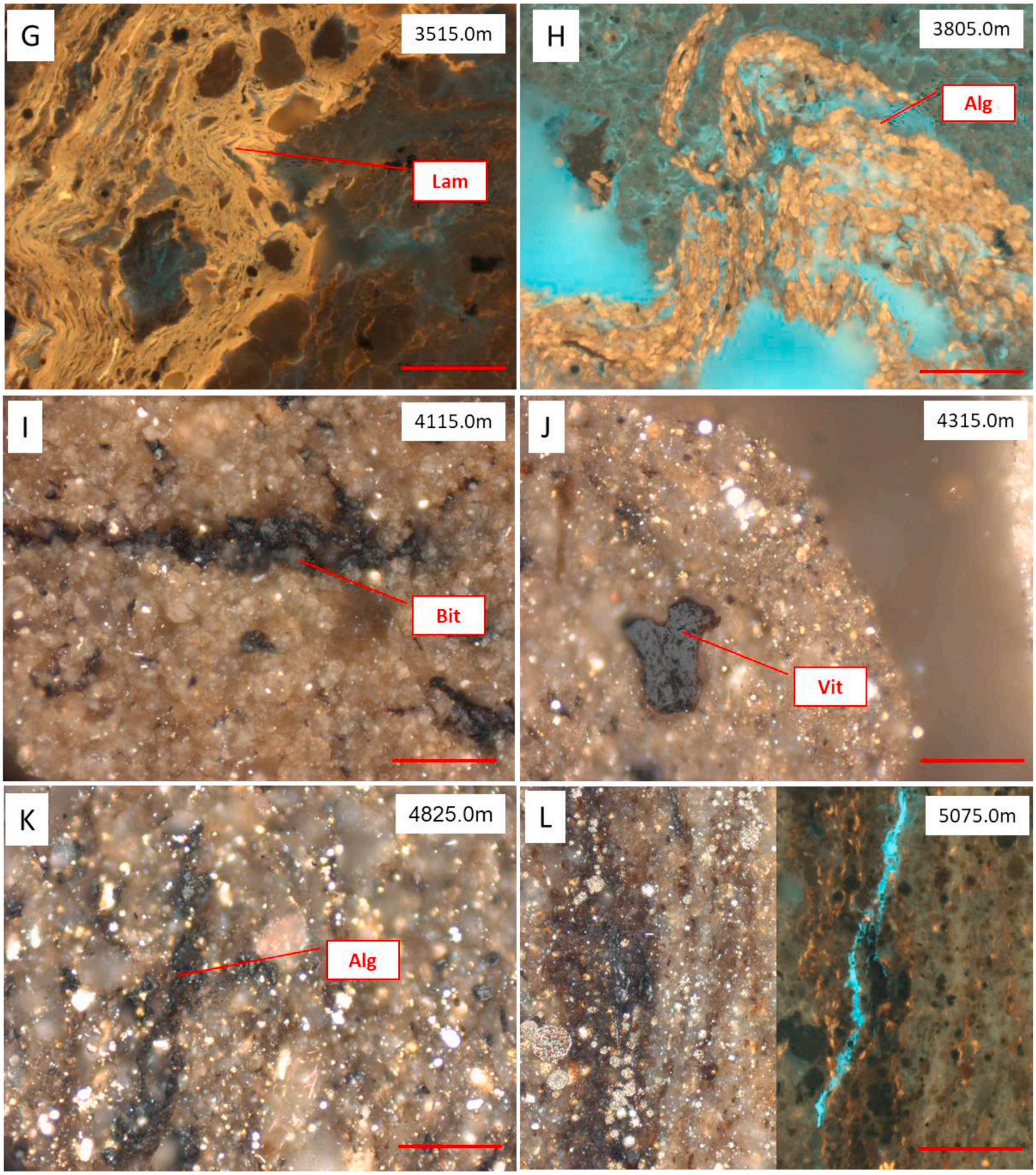

Fig. 5. (*continued*).

samples is consistent with early oil window maturity. The North Dana I-43 samples show similar oscillating OM types to the other wells, but the marine derived lamalginite macerals have been bituminized and do not fluoresce suggesting a high degree of thermal alteration (Hackley et al., 2018, Fig. 5I to L).

The maceral distribution data (relative volume%) applies the sum of the relative volume of primary and reworked vitrinite plus inertinite (V + I) versus the relative volume of liptinite macerals (L) as the two end members of the terrigenous influenced depositional environment versus marine. The relative volume of solid bitumen (B), observed exclusively in the North Dana I-43 well is indicative of the liptinite thermal conversion into solid bitumen at higher post oil thermal maturity (BRo = 1.10–1.16%; Table 3). These data used on a ternary plot (Fig. 6) show the strong influence of depositional environment and the oscillations in relative sea level have on the composition, preservation, and distribution of OM. The supply of terrigenous derived OM (V + I) decreases with the rise of relative sea level (Omura and Hoyanagi, 2004). Therefore, samples that plot closer to the (L) apex in Fig. 6 are mainly Type II oil prone OM and can be considered marine in origin. Conversely, when relative sea level is low the supply of terrigenous derived OM increases, these samples plot towards the (V + I) apex in Fig. 6. These observations occur regardless of the depth or age of the sediment and appear in a cyclical pattern throughout the Tithonian and Kimmeridgian. The North Dana I-43 samples show the same depositional environment observations, but the Type II OM (alginite) have been bituminized (B) due to higher thermal maturity (BRo = 1.10–1.16%) than the other samples.

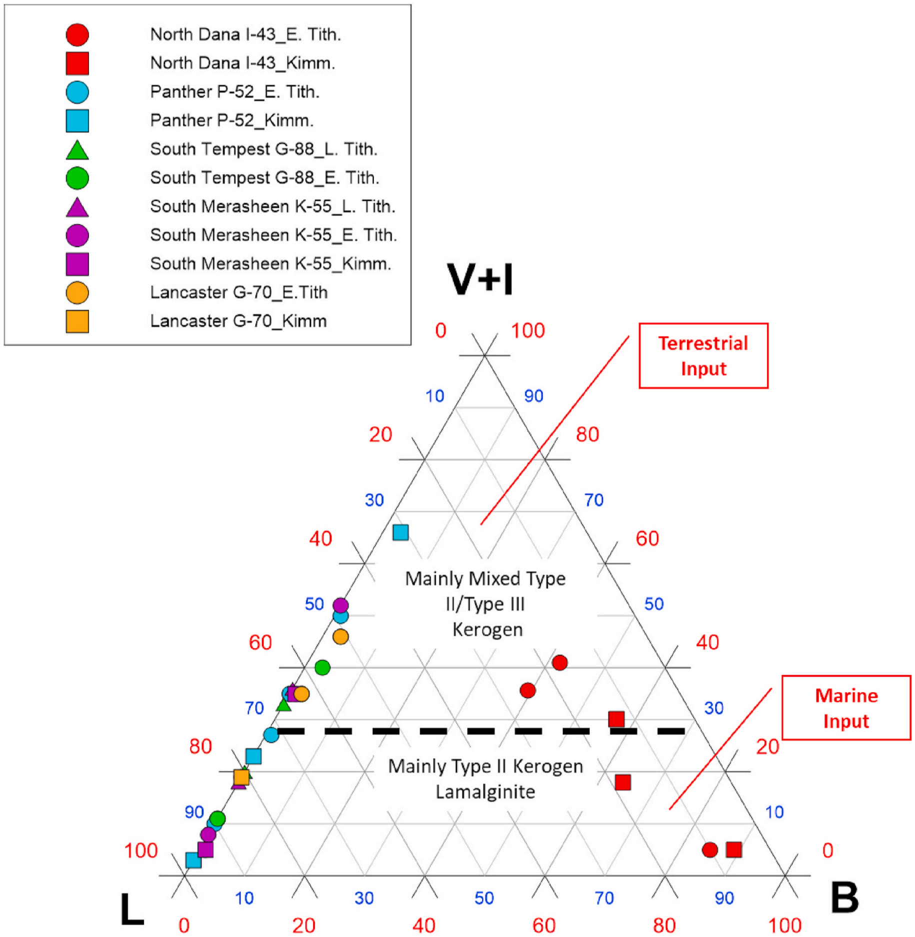

Fig. 6. Ternary plot showing vitrinite and inertinite (V + I) added together to represent terrestrial input and bitumen (B) and liptinite (L) represents marine input.

4.3. Thermal maturity

Selected representative examples of reflectograms show the Ro values for (i) vitrinite, and (ii) reworked vitrinite (Fig. 7). The dilution of terrigenous OM input resulting from proximity to deltaic sediment source is indicated by the abundant high reflective reworked/recycled vitrinite. It is the mixing and inclusion of these reworked/recycled vitrinite macerals that are responsible for the inconsistent multiple populations of thermal maturity parameters observed in the pyrolysis and measured %VRo data. Recycled vitrinite may have variable sources and have undergone multiple processes during transport such as oxidation and degradation of OM (e.g., Hartkopf-Froder et al., 2015; Synnott et al., 2017). North Dana I-43 is the only well with abundant solid bitumen, therefore North Dana I-43 reflectograms includes the measured bitumen reflectance (%BRo). Solid bitumen is derived from the decomposition (thermal cracking) of former oil or kerogen (Hartkopf-Froder et al., 2015). Solid bitumen can be utilized as an alternative maturity indicator and %BRo can be converted to equivalent 226 vitrinite reflectance (% VRoequ) using Equation (2) from Landis and Castano (1995). These values are reported in Table 3.

$$\%VR_{O_{equ}} = (BR_O + 0.41) / 1.09 \quad \text{(Eq. 1)}$$

Thermal maturity based on Tmax from the pyrolysis data is converted to %VRoequ using the calculation by Jarvie (2012) in equation (2) (Table 3).

$$\%VR_{O_{equ}} = (0.0180 \times T_{max}) - 7.16 \quad \text{(Eq. 2)}$$

Measured %VRo values (Table 3) show a wide range of thermal maturity from early oil window (%VRo = 0.62) to peak oil window (% VRo = 0.82) in South Merasheen K-55 and Panther P-52. The South Tempest G-88 and Lancaster G-70 wells show oil window maturity with %VRo ranging 0.72–0.79%. The North Dana I-43 well falls within the end of oil window to the onset gas window with %VRoequ ranging 1.10–1.16%. A strong positive logarithmic correlation ($R2 = 0.70$) exists between the relative volume distribution of liptinite group OM from the point count data to programmed pyrolysis HI values in the studied samples (Fig. 8). The increase in hydrocarbon potential (oil production) is hence directly related to occurrence and preservation of the liptinites in the samples representing the marine depositional environment. The hydrocarbon potential of samples decreases with the preservation of mainly terrigenous derived OM. North Dana I-43 shows the depletion of HI because of the conversion of liptinite to solid bitumen.

The hydrocarbon potential of the Jurassic-aged source rock intervals in the Central Ridge area is largely controlled by the oscillation of sea level in the depositional environment influencing the OM types preserved. The organic-rich lamalginites are related to the marine depositional environment that controls the OM production, accumulation, and preservation. The hydrocarbon generation potential of the oil prone Type II kerogen (i.e., lamalginite macerals) is good to excellent.

Since vitrinite is the main maceral used for determination of measured thermal maturity, the Type II lamalginites are not directly measured for %VRo by this method. Therefore, the thermal maturity of these macerals is not accurately represented in the reflectance data. Liptinite macerals show reflectance much less than vitrinite and posses autofluorescence when illuminated with ultra-violet or blue light (Pickle et al., 2017). Bright green to greenish yellow fluorescence colour is present in immature macerals up to the oil window while macerals with a fluorescence colour of yellow to orange to have a %VRo of 0.60–0.90%

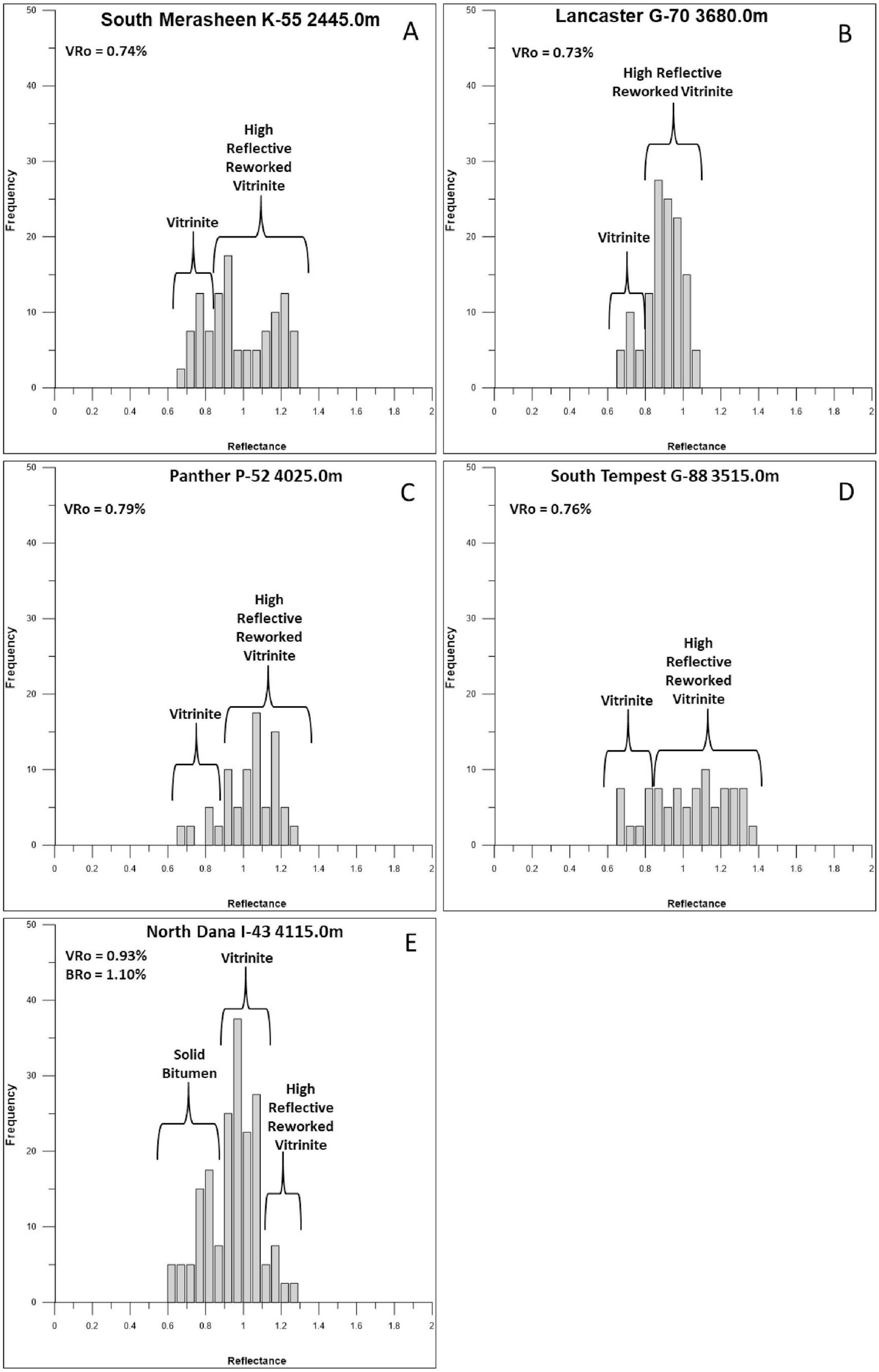

Fig. 7. Selected reflectograms showing the measured %VRo values and the macerals the data represents.

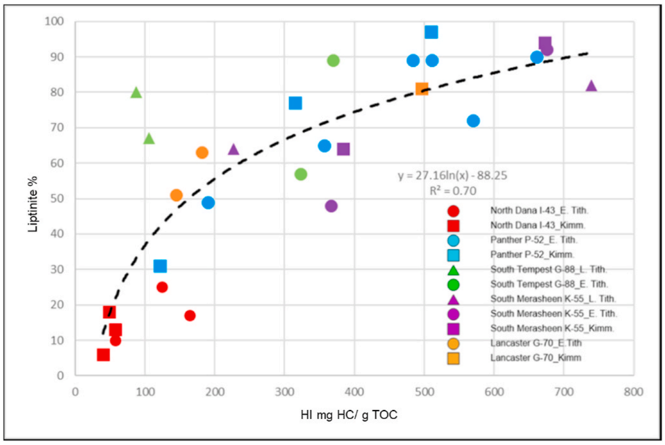

Fig. 8. Relationship between the relative volume of the liptinites in the sample versus measured hydrogen index (HI).

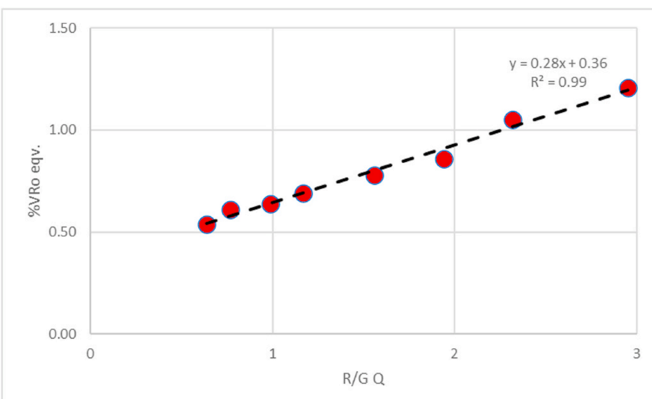

Fig. 9. Data modified from Inan et al. (2016). From this graph the thermal maturity of the Central Ridge samples can be estimated using the equation of the line.

(Pickle et al., 2017) indicating early to oil window maturity.

The Red/Green Quotient (Q) is the ratio of relative intensity at 650 nm to relative intensity at 500 nm (Teichmüller and Wolf, 1977) that shows a positive correlation with the degree of thermal maturity (Thompson-Rizer and Woods, 1987). Inan et al. (2016) used a method to estimate the thermal maturity of core samples taken from The Lower Silurian Qusaiba Hot Shales in Saudi Arabia. The thermal maturity historically reported on these source rocks, due to the lack of vitrinite preservation, can be conflicting due to different thermal maturity measurement methods used. The fluorescence properties R/G Q were measured on scattered alginites found in the Lower Silurian-aged samples. Using the linear equation ($y = 0.28x + 0.36$) from Inan et al. (2016), the thermal maturity can be extrapolated and used to estimate %VRo$_{equ}$ from the measured R/G Q from the fluorescing alginites found in the Central Ridge samples (Fig. 9). Panther P-52 and South Merasheen K-55 show immature to early oil window maturity (%VRo$_{equ}$ = 0.58–0.60%). South Tempest G-88 and Lancaster G-70 show early oil window maturity (% VRo$_{equ}$ = 0.61–0.66%) respectively.

Comparing thermal maturity data collected by both pyrolysis and organic petrology show different ranges of thermal maturity by depth (Fig. 10A to C). The mixing of terrigenous OM with marine derived OM can lead to misleading thermal maturity results in both Tmax derived %VRo and measured %VRo. These samples show the OM in these sediments to be immature to peak oil window maturity (Fig. 10A and B). Using the R/G Q converted to %VRoequ data, based on Inan et al. (2016), collected only on the fluorescing liptinite macerals, a more consistent thermal maturity trend can be seen (Fig. 10C).

5. Conclusion

This study shows organic geochemical and petrology results of drill cuttings samples taken from the Upper Jurassic Tithonian-aged and Kimmeridgian-aged source rocks intervals from five wells in the Central Ridge area offshore Newfoundland, Canada. Hydrocarbon potential is strongly related to depositional environment. The low hydrocarbon potential samples are related to the dilution by clastic terrigenous organic matter input due to proximity to deltaic sediment source. High reflective reworked/recycled vitrinite and inertinite are abundant in these sediments due to episodes of clastic dilution. Organic matter (OM)

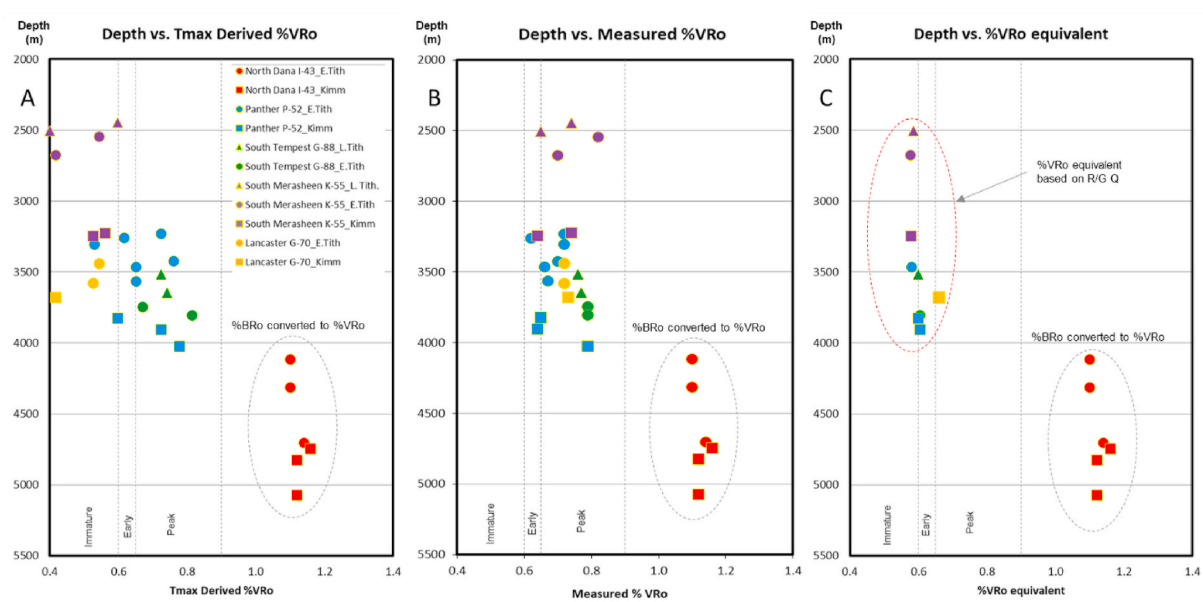

Fig. 10. A) Depth vs. Tmax derived %VRo showing thermal maturity to range from immature to peak oil window. Note North Dana I-43 samples are %BRo converted to %VRo. B) Depth vs. Measured %VRo showing similar thermal maturity to graph A. C) Depth vs. %VRo equivalent showing thermal maturity for these samples based on R/G Q values to be immature to early oil window.

can become altered in this depositional environment by becoming oxidized and degraded and as a result hydrogen index (HI) decreases while oxygen index (OI) increases. High hydrocarbon potential samples are limited to the organic-rich lamalginites and filamentous alginite related to deeper offshore marine depositional environments that controls the organic matter production, accumulation, and preservation. A combination of petrographic analytical techniques used in this study including maceral point counts and spectral data measured on fluorescing lamalginite macerals are key parameters to predicting thermal maturity. The oil generation potential of the samples with abundant lamalginite macerals is good to excellent in the Kimmeridgian-aged and in the Tithonian-aged samples.

Spectral R/G Q data for these macerals show thermal maturity to be appear immature to early mature. The dilution of higher reflectance and reworked/recycled vitrinite macerals, sourced from deltaic terrigenous input caused by sea level changes, is responsible for the multiple populations of %VRo and Tmax values in these samples. North Dana I-43 is in the deeper part of the section and is the only exception with the thermal maturity in the late oil to wet gas window (VRoequ = 1.10%). This study shows that using several geochemistry techniques, perhaps most importantly spectral data collected on fluorescing algal macerals, needs to be applied to understanding heterogenous mudrock intervals and the hydrocarbon potential of mudrock systems.

Contribution of authors

John B. Gordon, The conception and design of the study, Analysis and interpretation of data (organic petrology, geochemistry), Drafting the article or revising it critically for important intellectual content. Hamed Sanei, Interpretation of data (organic petrology, geochemistry), Revising the manuscript critically for important intellectual content. Omid H. Ardakani, Interpretation of data (organic petrology, geochemistry), Revising the manuscript critically for important intellectual content. Per K. Pedersen, Interpretation of data (depositional setting), Revising the manuscript critically for important intellectual content.

Declaration of competing interest

The authors declare the following financial interests/personal relationships which may be considered as potential competing interests: The following authors have affiliations with organizations with direct or indirect financial interest in the subject matter discussed in the manuscript: 1. John B. Gordon: University of Calgary. 2. Hamed Sanei: Aarhus University. 3. Omid H.: Ardakani Geological Survey of Canada. 4. Per K.: Pedersen University of Calgary.

Acknowledgments

We are extremely grateful to the Geological Survey of Canada for the use of their lab facilities as well as Husky Energy Inc. and Suncor Energy for supplying samples for this study. Many thanks to Wildcat Technologies for running our pyrolysis samples. We would also like to thank our editor, Dr. Tian Hui and our reviewers, Dr. Paul Hackley and one anonymous reviewer for their insightful and constructive comments.

References

Akande, S., Egenhoff, S., Obaje, N., Ojo, O., Olabisi, A., Erdtmann, B., 2012. Hydrocarbon potential of Cretaceous sediments in the Lower and Middle Benue Trough, Nigeria: insights from new source rock facies evaluation. J. Afr. Earth Sci. 64, 34–47.
BeicipFranlab, 2015. Offshore Newfoundland & Labrador Resource Assessment Flemish Pass Area NL15_01EN. An Integrated Project for: Nalcor Energy – Oil and Gas Inc. Department of Natural Resources, Government of Newfoundland and Labrador.
Bustin, R.M., 1988. Sedimentology and characteristics of dispersed organic matter in Tertiary Niger delta: origin of source rocks in a deltaic environment. AAPG (Am. Assoc. Pet. Geol.) Bull. 72, 277–298.
Carvajal-Ortiz, H., Gentzis, T., 2015. Critical considerations when assessing hydrocarbon plays using Rock-Eval pyrolysis and organic petrology data: data quality revisited. Int. J. Coal Geol. 125 (part A), 113–122.
Conford, C., 1998. Source rocks and hydrocarbons of The North sea. In: Glennie, K.W. (Ed.), Petroleum Geology of the North Sea. Blackwell, Oxford, pp. 376–462.
Cotterill, J.L., 1987. Well History Report Petro-Canada Lancaster G-70. Petro-Canada Internal Report (Unpublished).
Creaney, S., Allison, B.H., 1987. An organic geochemical model of oil generation in the Avalon/Flemish Pass sub-basins, east coast Canada. Bull. Can. Petrol. Geol. 35 (1), 12–23.
Dembicki, H., 2009. Three common source rock evaluation errors made by geologists during prospect or play appraisals. AAPG (Am. Assoc. Pet. Geol.) Bull. 93, 341–356.
Dewing, K., Sanei, H., 2009. Analysis of large thermal maturity datasets: examples from the Canadian Arctic Islands. Int. J. Coal Geol. 77 (3–4), 436–448.
DeSilva, N.R., 1999. Sedimentary basins and petroleum systems offshore Newfoundland and Labrador. In: Fleet, A.J., Boldy, S.A.R. (Eds.), Petroleum Geology of Northwest Europe: Proceedings of the Fifth Conference. The Geological Society, London, pp. 501–515.
Enachescu, M.E., Hogg, J.R., Fowler, M., Brown, D.E., Atkinson, I., 2010. Late Jurassic Source Rock Super-highway on Conjugate Margins of the North and Central Atlantic (Offshore East Coast Canada, Ireland, Portugal, Spain and Morocco), vol. 2. CM 2010-Abstracts.
Enachescu, M., 2012. Petroleum Exploration Opportunities in the Flemish Pass Basin. Call for Bids NL12-02, Parcel 1. http://www.nr.gov.nl.ca/nr/invest/call_bids_petro_exploration_enachescu%20.pdf.
Foster, D.G., Robson, A.G., 1993. Geological history of the flemish Pass Basin, offshore Newfoundland. AAPG (Am. Assoc. Pet. Geol.) Bull. 77, 588–609.
Fowler, M.G., Snowdon, L.R., Stewart, K.R., McAlpine, K.D., 1990. Rock-Eval/TOC Data from Nine Wells Located Offshore Newfoundland, vol. 2271. Geol. Surv. Can. Open File Rep, p. 72.
Fowler, M.G., Snowdon, L.R., Stewart, K.R., McAlpine, K.D., 1991. Rock-Eval/TOC Data from Five Wells Located within Jeanne d'Arc Basin, Offshore Newfoundland, vol. 2392. GeoL Surv. Can.Open File Rep, p. 41.
Fowler, M.G., McAlpine, K.D., 1995. The Egret member, a prolific kimmeridgian source rock from offshore eastern Canada. In: Katz, B.J. (Ed.), Petroleum Source Rocks. Casebooks in Earth Sciences. Springer, Berlin, Heidelber.
Fowler, M.G., Obermajer, M., Achal, S., Milovic, M., 2007. Results of Geochemical Analyses of an Oil Sample from Mizzen L-11 Well, Flemish Pass, Offshore Eastern Canada. Open-File Report - Geological Survey of Canada.
Gentzis, T., Carvajal-Orteiz, H., Ocubalidet, S.G., Wawak, B., 2017. Organic petrology characteristics of selected shale oil and shale gas reservoirs in the USA: examples from "the magnificent nine. Geology: Current and Future Development 1, 131–168.
Goodarzi, F., Haeri-Ardakani, O., Gentzis, T., Pedersen, P.K., 2019. Organic petrology and geochemistry of tournaisian-age albert formation oil shales, new brunswick, Canada. Int. J. Coal Geol. 205, 43–57.
Hackley, P.C., Araujo, C.V., Borrego, A.G., Bouzinos, A., Cardott, B., Cook, A.C., Eble, C., Flores, D., Gentzis, T., Gonçalves, P., Mendonça Filho, J.G., Hámor-Vidó, M., Jelonek, I., Kommeren, K., Knowles, W., Kus, J., Mastalerz, M., Menezes, T.R., Newman, J., Oikonomopoulos, I.K., Pawlewicz, M., Pickel, W., Potter, J., Ranasinghe, P., Read, H., Reyes, J., Rodriguez, G.D.L.R., Fernandes de Souza, I.V.A., Suarez-Ruiz, I., Sýkorová, I., Valentine, B.J., 2015. Standardization of reflectance measurements in dispersed organic matter: results of an exercise to improve interlaboratory agreement. Mar. Petrol. Geol. 59, 22–34.
Hackley, P.C., Valentine, B.J., Hatcherian, J.J., 2018. On the petrographic distinction of bituminite from solid bitumen in immature to early mature source rocks. Int. J. Coal Geol. 196, 232–245.
Hackley, P., Zhang, T., Jubb, A., Valentine, B., Dulong, F., Hatcherian, J., 2020. Organic petrography of Leonardian (Wolfcamp A) mudrocks and carbonates, Midland Basin, Texas: the fate of oil-prone sedimentary organic matter in the oil window. Mar. Petrol. Geol. 112.
Hartkopf-Fröder, C., Königshof, P., Littke, R., Schwarzbauer, J., 2015. Optical thermal maturity parameters and organic geochemical alteration at low grade diagenesis to anchimetamorphism: a review. Int. J. Coal Geol. 150 (151), 74–119.
Huang, Z., 1994. Predicted and measured petrophysical and geochemical characteristics of the Egret member oil source rock, Jeanne d'Arc basin, offshore eastern Canada. Mar. Petrol. Geol. 11, 294–306.
Inan, S., Goodarzi, F., Mumm, A.S., Arouri, K., Qathami, S., Arouri, A., Qathami, S., Ardakani, O.H., Inan, T., Tuwailib, A., 2016. The silurian Qusaiba Hot shales of Saudi arabia; an integrated assessment of thermal maturity. Int. J. Coal Geol. 159, 107–119.
Jarvie, D.M., 2012. Shale resource systems for oil and gas: Part 1 – shale oil resource systems. In: Breyer, J. (Ed.), Shale Reservoirs – Giant Resources for the 21st Century, vol. 97. AAPG Memoir, pp. 1–19.
Landis, C.R., Castano, J.R., 1995. Maturation and bulk chemical properties of a suite of solid hydrocarbons. Org. Geochem. 22 (1), 137–149.
Lafargue, E., Marquis, F., Pillot, D., 1998. Rock-Eval 6 applications in hydrocarbon exploration, production and soil contamination studies. Rev. Inst. Fr. Petrol 53 (4), 421–437.
Lowe, D.G., Sylvester, P.J., Enachescu, M.E., 2011. Provenance and paleodrainage patterns of upper jurassic and lower cretaceous synrift sandstones in the flemish Pass Basin, offshore Newfoundland, east coast of Canada. AAPG (Am. Assoc. Pet. Geol.) Bull. 95, 1295–1320.
Magoon, L.B., Hudson, T., Peters, K., 2005. Egret-Hibernia(!), a significant petroleum system, northern Grand Banks area, offshore eastern Canada. AAPG (Am. Assoc. Pet. Geol.) Bull. 89, 1203–1237.

Omura, A., Hoyanagi, K., 2004. Relationships between composition of organic matter, depositional environments, and sea-level changes in backarc basins, Central Japan. J. Sediment. Res. 74, 620–630.
Passey, Q.R., Bohacs, K., Esch, W.L., Klimentidis, R., Sinha, S., 2010. From Oil-Prone Source Rock to Gas-Producing Shale Reservoir - Geologic and Petrophysical Characterization of Unconventional Shale Gas Reservoirs. Society of Petroleum Engineers. https://doi.org/10.2118/131350-MS.
Peters, K.E., 1986. Guidelines for evaluating petroleum source rock using programmed pyrolysis. AAPG (Am. Assoc. Pet. Geol.) Bull. 70, 318–329.
Peters, K., Cassa, M., 1994. Applied Source Rock Geochemistry. AAPG Memoir, p. 60.
Peters, K., Xia, X., Pomerantz, A., Mullins, O., 2015. Geochemistry applied to evaluation of unconventional resources. In: Unconventional Oil and Gas Resources Handbook: Evaluation and Development. Elsevier, pp. 71–126.
Pickel, W., Kus, J., Flores, D., Kalaitzidis, S., Christanis, K., Cardott, B.J., Misz-Kennan, M., Rodrigues, S., Hentschel, A., Hamor-Vido, M., Crosdale, P., Wagner, N., 2017. Classification of liptinite – ICCP system 1994. Int. J. Coal Geol. 169, 40–61.
Pratt, L.M., 1984. Influence of paleoenvironmental factors on preservation of organic matter in middle cretaceous greenhorn formation, pueblo, Colorado. AAPG (Am. Assoc. Pet. Geol.) Bull. 68, 1146–1159.
Sanei, H., 2020. Genesis of solid bitumen. Sci. Rep. 10, 15595.
Sanei, H., Ardakani, O.H., Akai, T., Akihisa, K., Jiang, C., Wood, J.M., 2020. Core versus cuttings samples for geochemical and petrophysical analysis of unconventional reservoir rocks. Sci. Rep. 10, 7920.
Swift, J.H., Williams, J.A., 1980. Petroleum source rocks, Grand Banks area. In: Miall, A. D. (Ed.), Facts and Principles of World Petroleum Occurrence: Canadian Society of Petroleum Geologists Memoir 6, pp. 567–587.
Synott, D.P., Sanei, H., Dewning, K., Haeri-Ardakani, O.H., Pedersen, P.K., 2017. Insight into visible light spectrum changes with increasing reflectance in bituminite and inertinite macerals. Fuel 197, 201–208.
Teichmuller, M., 1973. Advances in organic geochemistry. In: Tissot, B., Bienner, F. (Eds.). Technip, Paris, pp. 319–407.
Teichmüller, M., Wolf, M., 1977. Application of fluorescence microscopy in coal petrology and oil exploration. J. Microsc. 109, 49–73.
Thompson-Rizer, C.L., Woods, R.A., 1987. Microspectrofluorescence measurements of coals and petroleum source rocks. Int. J. Coal Geol. 7, 85–104.
von der Dick, H., 1989. Environment of petroleum source rock deposition in the Jeanne d'Arc Basin off Newfoundland. In: Tankard, A.J., Balkwill, H.R. (Eds.), Extensional Tectonics and Stratigraphy of the North Atlantic Margins, vol. 46. AAPG Memoir, pp. 295–303.
Xiong, D., Azmy, K., Blamey, N., 2015. Diagenesis and origin of calcite cement in the Flemish Pass Basin sandstone reservoir (Upper Jurassic): implications for porosity development. Mar. Petrol. Geol. 70, 93–118.
Yang, S., Horsfield, B., 2020. Critical review of the uncertainty of Tmax in revealing the thermal maturity of organic matter in sedimentary rocks. Int. J. Coal Geol. 225.